An ontologically consistent MRI-based atlas of the mouse diencephalon

Charles Watson, Andrew L. Janke, Carlo Hamalainen, Shahrzad M. Bagheri, George Paxinos, David C. Reutens, Jeremy F.P. Ullmann

PII: S1053-8119(17)30456-1
DOI: http://dx.doi.org/10.1016/j.neuroimage.2017.05.057
Reference: YNIMG14069

To appear in: *NeuroImage*

Received date: 21 November 2016
Revised date: 1 May 2017
Accepted date: 27 May 2017

Cite this article as: Charles Watson, Andrew L. Janke, Carlo Hamalainen Shahrzad M. Bagheri, George Paxinos, David C. Reutens and Jeremy F.P Ullmann, An ontologically consistent MRI-based atlas of the mous diencephalon, *NeuroImage,* http://dx.doi.org/10.1016/j.neuroimage.2017.05.057

An ontologically consistent MRI-based atlas of the mouse diencephalon

Charles Watson[a,c,d*], Andrew L. Janke[a,b], Carlo Hamalainen[b], Shahrzad M. Bagheri[b], George Paxinos[d], David C. Reutens[a,b], Jeremy F.P. Ullmann[a,b,e]

[a]The Australian Mouse Brain Mapping Consortium, The University of Queensland, Brisbane, Australia.

[b]Centre for Advanced Imaging, The University of Queensland, Brisbane, Australia.

[c]Health Sciences, Curtin University, Perth, Western Australia, Australia.

[d]Neuroscience Research Australia and The University of New South Wales, Sydney, Australia.

[e]Department of Neurology, Boston Children's Hospital, Boston, MA, USA

[*]Indicates corresponding author: 14 Little High St, Fremantle WA 6160, Australia. +61 411 600 864. c.watson@curtin.edu.au

ABSTRACT

In topological terms, the diencephalon lies between the hypothalamus and the midbrain. It is made up of three segments, prosomere 1 (pretectum), prosomere 2 (thalamus), and prosomere 3 (the prethalamus). A number of MRI-based atlases of different parts of the mouse brain have already been published, but none of them displays the segments the diencephalon and their component nuclei. In this study we present a new volumetric atlas identifying 89 structures in the diencephalon of the male C57BL/6J 12 week mouse. This atlas is based on an average of MR scans of 18 mouse brains imaged with a 16.4T scanner. This atlas is available for download at www.imaging.org.au/AMBMC. Additionally, we have created an FSL package to enable nonlinear registration of novel data sets to the AMBMC model and subsequent automatic segmentation.

Abbreviations:

3N, oculomotor nucleus; 3PC, oculomotor nucleus, parvicellular part; 3V, third ventricle; 4N, trochlear nucleus ; ac, anterior commissure; acp, anterior commissure, posterior limb; AD, anterodorsal thalamic nucleus; AM, anteromedial thalamic nucleus; AMV, anteromedial thalamic nucleus, ventral part; AngT, angular thalamic nucleus; APT, anterior pretectal nucleus; APTD, anterior pretectal nucleus, dorsal part; APTV, anterior pretectal nucleus, ventral part; Aq, aqueduct; aur, auditory radiation; AV, anteroventral thalamic nucleus; AVDM, anteroventral thalamic nucleus, dorsolateral part; AVVL, anteroventral thalamic nucleus, ventrolateral part; B9, B9 serotonin cells; bic, brachium of the inferior colliculus; bsc, brachium or the superior colliculus; CA1, field CA1 of the hippocampus; CA2, field CA2 of the hippocampus; CA3, field CA3 of the hippocampus; cc, corpus callosum; chp, choroid plexus; CL, centrolateral thalamic nucleus; CM, central medial thalamic nucleus; cp, cerebral peduncle; csc, commissure of the superior colliculus; D3V, dorsal 3rd ventricle; DG, dentate gyrus; Dk, nucleus of Darkschewitsch; DLG, dorsal lateral geniculate nucleus; DpG, deep gray layer of the superor colliculus; DpWh, deep white later of the superior colliculus; DR, dorsal raphe nucleus; eml, external medullary lamina; EP, endopeduncular nucleus; Eth, ethmoid thalamic nucleus; F, nucleus of the field of Forel; f, fornix; fi, fimbria; fr, fasciculus retroflexus; Gem, gemini hypothalamic nucleus; GP, globus pallidus; hbc, habenular commissure; hif, hippocampal fissure; IAD, interanterodorsal thalamic nucleus; IAM, interanteromedial thalamic nucleus; ic, internal capsule; IF, interfascicular nucleus; IGL, intergeniculate leaflet; IMA, intermedullary thalamic nucleus; IMD,

intermediodorsal thalamic nucleus; InC, interstitial nucleus of Cajal; InCSh, interstitial nucleus of Cajal, shell region; InG, intermediate layer of the superior colliculus; InWh, intermediate white layer of the superior colliculus; IPF, interpeduncular fossa; IPC, interpeduncular nucleus, caudal part; IPR, interpeduncular nucleus, rostral part; isRt, isthmic reticular formation; IVF, interventricular foramen; JPLH, juxtaparaventricular part of lateral hypothalamus; LD, laterodorsal thalamic nucleus; LDDM, laterodorsal thalamic nucleus, dorsomedial part; LDVL, laterodorsal thalamic nucleus, ventrolateral part; LHb, lateral habenular nucleus; LHbM, lateral habenular nucleus, medial part; LP, lateral posterior thalamic nucleus; LPAG, lateral part of the periaqueductal gray; LPLC, lateral posterior thalamic nucleus, laterocaudal part; LPLR, lateral posterior thalamic nucleus, laterorostral part; LPMC, lateral posterior thalamic nucleus, mediocaudal part; LPMR, lateral posterior thalamic nucleus, mediorostral part; LT, lateral terminal nucleus (pretectum); Lth, lithoid nucleus; LV, lateral ventricle; MA3, medial accessory oculomotor nucleus; MCPC, magnocellullar nucleus of the posterior commissure; mes, mesencephalon; MD, mediodorsal thalamic nucleus; MDC, mediodorsal thalamic nucleus, central part; MDL, mediodorsal thalamic nucleus, lateral part; MDM, mediodorsal thalamic nucleus, medial part; MG, medial geniculate nucleus; MGD, medial geniculate nucleus, dorsal part; MGM, medial geniculate nucleus, medial part; MGV, medial geniculate nucleus, ventral part; MHb, medial habenular nucleus; ml, medial lemniscus; mlf, medial longitudinal fasciculus; mp, mamillary peduncle; MPT, medial pretectal nucleus; MT, medial terminal nucleus; mt, mammillothalamic tract; ns, nigrostriatal tract; Op, optic nerve layer of the superior colliculus; OPC, oval paracentral thalamic nucleus; OPT, olivary pretectal nucleus; opt, optic tract; OT, nucleus of the optic tract; p1, prosomere 1; p1Rt, prosomere 1 reticular formation; p2, prosomere 2; p3, prosomere 3; Pa, paraventricular hypothalamic nucleus,; PaF, parafascicular thalamic nucleus; PAG, periaqueductal gray; PaPo, paraventricular hypothalamic nucleus, posterior part; PaR, pararubral nucleus; PaXi, paraxiphoid nucleus; PBP, parabrachial pigmented nucleus of the ventral tegmental area; PC, paracentral thalamic nucleus; PCom, nucleus of the posterior commissure; PF, parafascicular thalamic nucleus; PH, posterior hypothalamus; PIF, parainterfascicular nucleus of the VTA; PIL, posterior intralaminar thalamic nucleus; pm, principal mammillary tract; PN, paranigral nucleus; Po, posterior thalamic nuclear group; PoT, posterior thalamic nuclear group, triangular part; PP, peripeduncular nucleus; PR, prerubral field; PrC, precommissural nucleus; PrEW, pre-Edinger-Westphal nucleus; PrG, pregeniculate nucleus of the prethalamus; PSTh, parasubthalamic nucleus; PT, paratenial thalamic nucleus; PTg, peduncular tegmental nucleus; PV, paraventricular thalamic nucleus; PVA, paraventricular thalamic nucleus, atnerior part; PVP, paraventricular thalamic nucleus, posterior part; Re, reuniens thalamic nucleus; REth, retroethmoid nucleus; Rh, rhomboid thalamic nucleus; RI, rostral interstitial nucleus; RLi, rostral linear nucleus; RM, retromamillary nucleus; RMC, red nucleus, magnocellular part; RPC, red nucleus, parvicellular part; RPF, retroparafascicular nucleus; RRe, retroreuniens nucleus; RRF/A8, retrorubral field and A8 dopamine cells ; Rt, reticular nucleus (prethalamus); Sag, sagulum nucleus; SC, superior colliculus; Sc, scaphoid nucleus; scp, superior cerebellar peduncle; SG, supragenicuiate nucleus; sm, stria medullaris; SNC, substantia nigra, compact part; SNCD, substantia nigra, compact part, dorsal tier; SNL, substantia nigra, lateral part; SNR, substantia nigra, reticular part; sox, supraoptic descussation; SPF, subparafascicular thalamic nucleus; SPFPC, subparafascicular thalamic nucleus, parvicellular part; st, stria terminalis; STh, subthalamic nucleus; str, superior thalamic

radiation; Su3, supraoculomotor periaqueductal gray; Su3C, supraoculomotor cap; Sub, submedius thalamic nucleus; SubB, subbrachial nucleus; SubG, subgeniculate nucleus of the prethalamus (ventrolateral nucleus); SuG, superficial gray layer of the superior colliculus; Te, terete hypothalamic nucleus; TG, tectal gray; TS, triangular septal nucleus; VA, ventral anterior thalamic nucleus; vhc, ventral hippocampal commissure; VL, ventrolateral thalamic nnucleus; VLi, ventral linear nucleus; VM, ventromedial thalamic nucleus; VPL, ventral postereolateral thalamic nucleus; VPM, ventral postereomedial thalamic nucleus; VPPC, ventral posterior thalamic nucleus; VRe, ventral reuniens thalamic nucleus; VTA, ventral tegmental area; VTAR, ventral tegmental area, rostral part; vtgx, ventral te; Xi, xiphoid nucleus; ZI, zona incerta; ZIC, zona incerta, central part; ZID, zona incerta, dorsal part; ZIR, zona incerta, rostral part; ZIV, zona incerta, ventral part

KEYWORDS: thalamus, pretectum, prethalamus, segmentation, diencephalon, MRI

1. INTRODUCTION

The anatomical status of the diencephalon has undergone a major revision since the discovery of gene targeting in mice. The traditional concept of the diencephalon included the thalamus, hypothalamus, subthalamus, and epithalamus; however, recent studies of developmental gene expression have challenged this assembly (Puelles et al., 2013; Watson et al., 2017), and the revised view of the diencephalon excludes the hypothalamus and the subthalamic nucleus. The reason for this is that the hypothalamus (of which the subthalamic nucleus is a part) is a complete segment of the forebrain, with alar and basal components, and completely distinct from the remainder of the diencephalon. The developing diencephalon therefore lies between the hypothalamus and midbrain; it consists of three segmental units called prosomeres, each of which has alar and basal components. The relationship between the three diencephalic prosomeres and surrounding structures is shown diagramatically in Figures 1 and 2, in which the diencephalic and neighbouring nuclei are outlined in a series of drawings of sagittal sections of mouse brain. The main part of the diencephalon is the thalamus, and Figure 3 is a diagrammatic view of the main groups of thalamic nuclei.

Prosomere 1 is the most caudal of the prosomeres and abuts the midbrain. It is made up of the pretectal nuclei and nuclei associated with the posterior commissure, and a number of nuclei previously classified as part of the midbrain. Like each of the diencephalic prosomeres, prosomere 1 forms a complete segment from the roof plate to the pial surface of the floor plate of the developing brain (Puelles et al., 2012b). Prosomere 2 includes the nuclei of the thalamus, including the habenula. It is the largest part of the diencephalon in mammals. It lies caudal to prosomere 3 and rostral to prosomere 1. An extensive two-volume monograph on the comparative anatomy of the mammalian thalamus by Jones (2007) shows that the mouse thalamus is similar to that of other placental mammals in all major respects. Conventional atlases of the mouse brain delineate about 50 distinct nuclei in the thalamus (Paxinos and Franklin, 2013; Watson and Paxinos, 2010). These nuclei can be organized into seven primary subdivisions, named the anterior, medial, lateral, ventral, posterior, midline, and

intralaminar groups. Prosomere 3 contains the nuclei of the prethalamus, including the reticular nucleus, the pregeniculate nucleus (formerly ventral lateral geniculate), and the zona incerta. The prosomere 3 nuclei contain many GABAergic neurons, whereas in the mouse GABA neurons are prominent in only a single prosomere 2 nucleus (the dorsal lateral geniculate nucleus).

Experimental investigations into neurological conditions affecting the diencephalon in animal models are mainly focused on the C57BL mouse because of the availability of extensive gene targeting data in this strain. Recently, there has been an increase in the number of studies investigating the mouse thalamus using functional, structural, and diffusion-weighted imaging (DWI) techniques to examine neurological disorders and map brain connectivity (Ferris et al., 2014; Keifer et al., 2015; Maheswaran et al., 2009; Malkova et al., 2014; Nessler et al., 2007; Richards et al., 2014; Shu et al., 2013). However, these studies have relied upon manual segmentation of the diencephalon or have used atlases that identify only a limited number of diencephalic structures (Dorr et al., 2008; Kovacevic et al., 2005; Ma et al., 2005; MacKenzie-Graham et al., 2004; Ullmann et al., 2012; Ullmann et al., 2014; Ullmann et al., 2013). In response to this limitation, we have endeavoured to create a comprehensive probabilistic atlas of the C57BL/6J mouse diencephalon. A feature of this atlas is that it is consistent with contemporary views on mammalian brain ontology based on developmental gene expression (Puelles et al., 2013; Watson et al., 2017).

2. MATERIALS AND METHODS

2.1 *C57BL/6J mouse brain preparation and magnetic resonance imaging*

Eighteen C57BL/6J mice (male, 12 week old) were perfused and fixed with 4% paraformaldehyde and 0.1% Magnevist® (gadopentetate dimeglumine, Bayer HealthCare Pharmaceuticals Inc., Wayne, NJ, USA) in phosphate buffer (PB). Brains were extracted and incubated in 0.1% Magnevist/PB for 4 days, placed in Fomblin (Solvay Solexis, Milan, Italy) and imaged on a 16.4T (89mm bore diameter) Bruker micro-imaging system (Bruker Biospin, Karlsruhe, Germany) using a 15 mm SAW coil (M2M Imaging, USA). MRI data were acquired using a 3D gradient echo sequence with a repetition time = 50ms, echo time = 12 ms, flip angle = 30°, 82 KHz spectral bandwidth, field of view = 2.1 x 1.05 x 0.75 cm, matrix = 700 x 350 x 250, 8 averages, resulting in a total acquisition time of 5 h 15 mins. There was no zero filling. This protocol produced T_2*-weighted images at 30 μm isotropic resolution.

2.2 *Minimum deformation model creation*

Images were placed in the stereotaxic coordinate space and a symmetric model was created using a recursive non-linear hierarchical fitting strategy (Janke and Ullmann, 2015; Ullmann et al., 2015). Briefly, the fitting strategy consisted of 3 linear fits to the evolving internal model followed by a hierarchical series of non-linear grid transforms. The fitting uses smoothed data with a 3D FWHM of half the step size. Twenty iterations at each fitting stage were performed using the ANIMAL algorithm. Interpolation resulted in a model with 15 μm^3 isotropic voxels. For a detailed description of the model creation see Janke and Ullmann (2015).

2.3 *Interpolation of tracings*

To interpolate the tracings we used a modified version of a previously published morphological smoothing algorithm (Albu et al., 2008). This algorithm was

developed for interpolating tracings of single structures such as the liver. In our implementation, each structure was first interpolated in isolation of other structures. However, this occasionally produced structures with overlapping boundaries. To resolve overlapping components, a heuristic approach was used that gave scores to each component based on its relative size and size of the overlapping portion. Conflicts were then resolved on a per-component basis by erasing the overlapping area from the losing component. As part of this process small holes in the traced volume were filled from the closest adjacent structure. As can be seen from the reconstructions in the out of plane directions (Fig 4) this results in a smooth set of anatomical labels.

2.4 *Anatomical delineation of parts of the diencephalon*

The major anatomical features of the diencephalon were primarily identified on the coronal sections of the model by anatomical experts (CW, GP, and JFPU). CW and GP are authors of a number of highly cited rodent brain atlases (Paxinos and Franklin, 2013); Paxinos and Watson, 2014; Paxinos et al., 2009; Watson and Paxinos, 2010) and JFPU is experienced in the development of MRI-based atlases of vertebrates (Ullmann et al., 2010; Ullmann et al., 2015; Ullmann et al., 2010b). The operational criteria for defining anatomical features were defined in terms of differences in signal intensity and their location with reference to anatomical landmarks.

The diencephalon was segmented into major regions and subregions using the parcellation scheme of Paxinos and Franklin (2013) and following the ontology outlined by Puelles et al. (2013). In a few cases our parcellation was more conservative than in the atlas, because in some cases the boundaries of sub-regions could not be clearly defined. In such cases, we combined the adjacent sub-regions. Structures were then segmented according to the operational criteria using vector-based segmentation performed on a Cintiq tablet (Wacom Company Ltd, Vancouver, USA). The complete data set was then exported to Amira (FEI, Hillsboro, Oregon) where structural boundaries were checked and corrected in the three orthogonal planes by JFPU and CW. The nomenclature and abbreviations used here were taken from Paxinos and Franklin (2013) and the color palette is based on that used in previous mouse brain atlases from our group. Smoothed three-dimensional surface reconstructions were created in Amira. Average image intensities were computed by first normalising the intensity values in the model to lie between 0 and 100 via percent critical thresholding of the intensity histogram for the entire image. In our case, cutoffs of 0.1% and 99.9% were used. The signal intensity across the structures of interest was then averaged. The volumes of individual structure were computed in model space from the delineated areas.

2.5 *FSL Package*

To facilitate the use of the atlas, we have created a FSL package for automatic model based segmentation based upon linear and nonlinear registration. FSL is a large library of analysis tools for MRI, DWI, and functional magnetic resonance imaging (Jenkinson et al., 2012). For human brain studies, FSL provides users with a configuration file (i.e. *T1_2_MNI152_2mm.cnf*) that can be used for non-linear registration of a human brain T1-weighted MRI to the MNI152 template (Andersson et al., 2010; Jenkinson et al., 2012). Some of the suggested parameters in the

AMBMC configuration file are derived from the existing MNI152 configuration file and then scaled appropriately to be applicable to mouse brain MR image registration.

One of the most important parameters is the *warpres*, which represents the image's warp resolution in mm, in three directions (x-, y- and z-axis) (Andersson et al., 2010). In the MNI152 configuration file, it is suggested to use the *warpres* of 10 mm in all directions, where the individual MRI is approximately 150 x 150 x 150 mm. This means that 15 control points (knots) are considered to be appropriate in that context. The mouse brain MR images in our research are roughly 10 x 15 x 7 mm. Consequently, in order to have 15 knots for controlling the warp field in the context of our work, a *warpres* of 0.66 x 1 x 0.46 mm is suggested. The same applies to the *biasres* parameter, which according to Andersson et al. ((2010) denotes the bias field resolution, and is only relevant when the intensity-mapping model (*intmod* parameter) is set to *local_linear* or *global_non_linear_with_bias* or *local_non_linear*. Therefore, a *biasres* of 3 x 5 x 2 mm is suggested in the AMBMC configuration file.

The other two important parameters are *infwhm* and *reffwhm*, which represent the FWHM (Full Width at Half Maximum) of the Gaussian smoothing kernel (in mm) for the input and the reference image, respectively (Andersson et al., 2010). As advised in the MNI152 configuration file, the values for both the FWHM parameters are usually about 3 times the image resolution at the highest level of subsampling. These values are then decreased gradually at the lower subsampling levels. Accordingly, use of *infwhm=0.18,0.15,0.12,0.09,0.06,0* and *reffwhm=0.06,0.06,0.03,0.03,0,0* are advised in the AMBMC configuration file, where a subsampling scheme of *subsamp=4,4,2,2,1,1* is applied. It should be noted that it is usually suggested to smooth the reference image less than the input image at each subsampling level, where the reference image is an averaged template image.

3. RESULTS

We have mapped the parts of the diencephalon on a series of coronal slices from the MR mouse brain average set. We have selected eight of these slices for presentation of our findings (Figs 5-8). In defining the boundaries of diencephalic structures, we approached the process of segmentation in a series of steps. First we identified the major fiber bundles that bound the region; these include the stria medularis, internal capsule, cerebral peduncle, optic tract, and the fibria of the fornix. Next we recorded the outline of fiber bundles within the diencephalon that stand out in MR images; these include the mamillothalamic tract, the fornix, the fasciculus retroflexus, the medial lemniscus, the internal medullary lamina, the external medullary lamina, the superior thalamic radiation, and the posterior commissure. Finally we outlined the position of certain nuclei that display distinctive contrast patterns defining them from their neighbours; these include the anterodorsal thalamic nucleus, the reticular nucleus, the zona incerta, the dorsal lateral geniculate nucleus, the pregeniculate nucleus, the ventromedial nucleus, and the medial habenula. Finally, we delineated the remaining diencephalic structures with reference to the histological mouse brain atlas of Paxinos and Franklin (2013). This last stage was the most difficult, since some structures do not have a distinct contrast pattern and had to be outlined by interpolation in relation to neighbouring structures that can be more confidently identified.

3.1 *Identifying the individual nuclei of the diencephalon in this MR atlas*
The identification of the nuclei of the diencephalon presented here follows the comprehensive monograph on the mammalian thalamus of Jones (2007) in all major respects, except that Jones did not explicitly recognize the three prosomeric subdivisions of the diencephalon. In this section, the nuclei of the diencephalon are identified in relation to Figures 5-8. We have prepared a protocol to assist with the identification of diencephalic nuclei in MRI images of mammalian brains, and we have included it in supplementary material.

3.1.1 *Nuclei of the prethalamus (prosomere 3)*
The largest prethalamic nucleus are the reticular nucleus and the zona incerta. In the sagittal images in Figures 1 and 2 these two nuclei can be seen to form a cup around the rostral pole and ventral border of the thalamus. In the coronal MR images (Figs 5-7), the reticular nucleus is bordered laterally by the internal capsule, and medially by a dense line that separates it from the anterior group (Fig 5). In more caudal sections (Figs 5B-7A), it is bordered medially by the ventral tier nuclei. At the level of the rostral pole of the dorsal lateral geniculate (Fig 5), the reticular nucleus is replaced by the pregeniculate nucleus, now named the ventral lateral geniculate Paxinos and Watson, 2014). The pregeniculate nucleus contains a dark vertical stripe in coronal sections, which forms an outstanding landmark (Figs 7B, 8A). The ventromedial tip of the reticular nucleus is continuous with the zona incerta (Figs 5-7A). In rostral sections (Fig 5), the zona incerta appears very pale, but it is darker in more caudal sections, where it is divided into dorsal and ventral parts (Figs 7B, 8A). The subgeniculate nucleus is interposed between the pregeniculate and cerebral peduncle in Fig 8A.

3.1.2 *Nuclei of the thalamus (prosomere 2)*
Anatomical subdivision of the thalamus is traditionally based on the position of two fiber sheets - the internal and external medullary laminae. Medial to the internal medullary lamina is the mediodorsal complex. Between the two medullary laminae are the dorsal and ventral tier nuclei. Rostrally, where the internal medullary lamina disappears, the anterior group occupies the position held by the mediodorsal complex in the middle of the thalamus. Associated with internal meduallary lamina are the intralaminar nuclei. Along the medial border of the thalamus are the midline nuclei. The ventral tier nuclei are the ventral anterior, ventral lateral, and ventral posterior nuclei. The dorsal tier nuclei are the lateral dorsal and lateral posterior nuclei. Caudally, the main ventral tier nuclei are replaced by the posterior nuclear group, the medial geniculate nucleus, and the dorsal lateral geniculate nucleus. The expanded caudal extension of the intralaminar group is the parafascicular nucleus. The relationship between the major thalamic nuclear groups is shown diagrammatically in Figure 3.

The *anterior group of thalamic nuclei* is made up of the anterodorsal, anteroventral, and anteromedial nuclei. The anterior nuclei lie between the reticular nucleus and the ventral anterior nucleus laterally and the stria medullaris, parataenial nucleus, and the mediodorsal nuclei medially. The interanterodorsal nucleus forms a curved dark band at the medial edge of the anterior group, roughly parallel to the dark band of the external medullary lamina, which separates the anterior group from the reticular nucleus of the prethalamus (Fig 5A). The dorsal tip of the dark band of the

interanterodorsal nucleus joins a very light triangular area occupied by the anterodorsal nucleus. The anteroventral nucleus lies ventrolateral to the anterodorsal nucleus at most coronal levels (Figs 5A, 6B). The anteromedial nucleus lies ventromedial to the anteroventral nucleus. It is a large nucleus that continues medially as the interanteromedial nucleus. The division between the anteroventral nucleus and the anteromedial nucleus is not always distinct, but the dorsomedial part of is distinctly lighter than the anteromedial nucleus.

The *dorsal tier nuclei* of the thalamus are the dorsal lateral nucleus and the lateral posterior nucleus. The dorsal lateral nucleus occupies a light area dorsal to the anteroventral nucleus where it forms a characteristic dome on the dorsal margin of the anterior pole of the thalamus (Fig 5A). More caudally the ventrolateral and dorsomedial parts of the lateral dorsal nucleus can be distinguished (Figs 5B-7A). In Figure 7A, the caudal pole of the ventrolateral part of the lateral ventral nucleus separates the lateral posterior thalamic nucleus from the rostral pole of the dorsal lateral geniculate, which appears very light. The lateral part of the lateral posterior nucleus straddles the dark superior thalamic radiation. The medial border of the lateral posterior nucleus abuts the central lateral nucleus rostrally and the anterior pretectal nucleus more caudally (Figs 7A, 8A)

The *ventral tier nuclei* of the thalamus include the ventral lateral, ventral posterior and ventral medial nuclei. The dorsal lateral geniculate and medial geniculate are usually considered to be caudal extensions of the ventroposterior group, but we will consider them under a separate heading. The ventrolateral group includes the ventral anterior nucleus (Fig 6A) and the ventrolateral nucleus (Figs 6A-7B), but can be considered to extend ventromedially into the ventromedial nucleus (Figs 5A-7B), and the submedius nucleus (Figs 5B-7A). The ventrolateral nucleus mainly lies medial to the rostral ventroposterior nucleus. The rostral part of the ventrolateral nucleus overlaps with the ventral anterior nucleus. The ventral anterior nucleus forms a lighter strip lateral to the anteroventral nucleus. Medial to ventrolateral nucleus are components of the intralaminar group and the anteromedial nucleus. The medium to light density of the ventrolateral nucleus is very similar to that of its dorsal neighbour, the posterior nucleus medial part (Fig 7A). The ventromedial nucleus forms a dark triangular or tear-drop shaped area (Figs 7A-8A); it is continuous caudally with the fibers of the superior cerebellar peduncle (Fig 8B). The submedius nucleus is a prominent, round group of cells medial to the ventromedial nucleus, close to the mamillothalamic tract (Figs 5B-7A). The main components of the ventroposterior group are the ventroposterior medial and the ventroposterior lateral nucleus, which receive somatosensory input from the head and the limbs and trunk, respectively. The ventroposterior lateral and ventroposterior medial nuclei appear relatively dark in Figs 6B-7B and there is a sharp border between the medial border of the ventroposterior medial and the much lighter profiles of the ventrolateral nucleus and the posterior nucleus medial part. The ventroposterior lateral nucleus, which is a little darker than the ventroposterior medial, is separated from the reticular nucleus by the very dark band of the external medullary lamina (Figs 6A-7A). The caudal half of the ventroposterior medial nucleus is continuous medially with the ventral posterior nucleus parvicellular part (Fig 7B), which receives gustatory and autonomic afferents (see Paxinos and Watson, 2014). The ventroposterior nucleus parvicellular part is in turn continuous caudally with a lighter patch named the subparafascicular nucleus parvicellular part (Fig 8A).

The lateral and medial geniculate nuclei. Although it is developmentally and functionally part of the ventral tier, the dorsal lateral geniculate nucleus occupies a dorsal position in the adult mouse thalamus, situated between the lateral posterior nucleus and the pregeniculate nucleus (Fig 8). Between the dorsolateral geniculate and the pregeniculate nucleus there is a distinct layer of cells called the intergeniculate leaf (Fig 8), which is developmentally part of prosomere 3 (Puelles et al., 2012b). The surface of the dorsal lateral geniculate nucleus is covered by the dark band of the optic tract. The medial geniculate nucleus is also considered to be a member of the ventral tier group, but it is displaced caudally to form the caudal pole of the thalamus, level with the rostral pole of the superior colliculus of the midbrain (Fig 8B). It is important to note that the medial geniculate is always separated from the midbrain by intervening parts of prosomere 1, mainly the anterior pretectal nucleus. Within the medial geniculate nucleus there are ventral, dorsal, and medial subdivisions (Fig 8B). Between the rostral pole of the medial geniculate and the caudal pole of the ventroposterior nucleus is a dark patch that has not previously been identified in mouse brain atlases. On the basis of anterograde tracing studies presented in the Allen Institute Website (Website: © 2015 Allen Institute for Brain Science. Allen Mouse Brain Connectivity Atlas [Internet]; Oh, S.W. et al., 2014); available from: http://connectivity.brain-map.org.), we believe that it is formed by the fibers projecting from the medial geniculate to the auditory cortex; we have labeled these fibers the auditory radiation (‘aur’ - Fig 8A).

The *medial nuclear group* includes the three subnuclei of the medial dorsal nucleus, the intermediodorsal nucleus, and the parataenial nucleus. The medial dorsal nucleus is bordered laterally and ventrally by the intralaminar nuclear group. The intermediodorsal nucleus is very light, but the remainder of the medial dorsal nucleus is made up of dark and light areas, which generally coincide with the medial, central, and lateral subnuclei defined in Nissl preparations (Paxinos and Franklin, 2013). Between the intermediodorsal nucleus and the habenular complex is a very light area occupied by the paraventricular nucleus. The parataenial nucleus forms a dark oval profile that is embedded in the rostral pole of the mediodorsal nucleus (Fig 5A).

The *intralaminar nuclei* are named for their association with the internal medullary lamina. They are the central lateral, paracentral, and central medial nuclei. The central lateral and paracentral nuclei are light in density compared to the lateral part of the medial dorsal nucleus, but the central medial nucleus is generally darker (Figs 5A-7A). The parafascicular nucleus represents a huge caudal expansion of the intralaminar group. It lies alongside the fasciculus retroflexus, and occupies a large area between the posterior nucleus medial part (laterally) and the periaqueductal gray (medially) (Figs 7B, 8A). The rostral pole of the parafascicular nucleus merges with the caudal pole of the paracentral nucleus. Between the most ventral extension of the anterodorsal nucleus and the parataenial nucleus is a dark patch representing the central medial nucleus (Fig 5A). Ventral to the central medial nucleus is a light band of the interanteromedial thalamic nucleus (Fig 5B). Ventral to the interanteromedial nucleus are the small rhomboid nucleus and the larger reuniens nucleus. The latter consists of a light central region and a region of dark patches laterally, called the ventral reuniens nucleus (Figs 5-7B). The xiphoid and paraxiphoid nuclei (which belong to prosomere 3 and not prosomere 2) are ventral to the light region of the reuniens nucleus, and are darker than the reuniens nucleus (Figs 5-7A).

The midline nuclei of the thalamus are a heterogeneous group that can be defined in different ways. For example, some authors choose to include in this group the extensions of paired thalamic nuclei that cross the midline, such as the interanteromedial and the intermediodorsal, and the midline part of the central medial nucleus. We prefer to classify these crossing nuclei with their larger lateral extensions. We have taken a simple approach by including in this group only nuclei which sit in the midline and that do not have lateral extensions. These nuclei are, from dorsal to ventral, the paraventricular nucleus, rhomboid nucleus, reuniens nucleus, and xiphoid nucleus (Figs 5-8A). We note however that the rhomboid nucleus lies adjacent to the central medial nucleus, and is considered by many to belong to the intralaminar-parafascicular group on the basis of cytoarchitecture and connections (Jones, 2007). Both the xiphoid and reuniens nuclei have small lateral extensions, the paraxiphoid and retroreuniens nuclei respectively (Figs 5B-7A). The paraventricular nucleus is mostly applied to the dorsal ependymal surface of the thalamus, ventral to the dorsal recess of the third ventricle (Figs 5-6). The rostral pole is named the anterior paraventricular nucleus (Fig 5), and the caudal pole is named the posterior paraventricular nucleus (Fig 7B).

The *posterior nuclear group of the thalamus* lies mainly between the parafascicular thalamic nucleus and the ventroposteromedial nucleus. The main components of this group include the medial posterior nucleus, the ethmoid nucleus, the retroethmoid nucleus, the posterior intralaminar nucleus, and the triangular posterior nucleus (Figs 7B-8). The central part of the large medial posterior nucleus has a triangular shape, with the dorsal border formed by the lateral posterior nuclei (Fig 7B). The caudal part of the posterior nucleus medial part is squeezed between the anterior pretectal nucleus medially and the medial geniculate laterally (Fig 8A). The caudal pole of the medial posterior nucleus is continuous dorsally with the triangular nucleus of the posterior complex and the posterior intralaminar nucleus ventrally. The ethmoid and retroethmoid nuclei occupy a position between the caudal pole of the parafascicular nucleus and the medial posterior nucleus (Fig 8A). In diagrams in the histological atlas of (Paxinos and Franklin, 2013), the dorsal part of the ethmoid nucleus is separated from the lateral border of the anterior pretectal nucleus by two small nuclei, the scaphoid nucleus and the posterior limitans nucleus, but we could not confidently identify these nuclei in MR slices.

The habenula forms a distinctive rostrocaudal strip along the dorsomedial corner of the thalamus, closely applied to the stria medullaris (Figs 5-7). The habenula nuclei stand out clearly in MR images; the medial habenular nucleus is very light compared to the lateral habenular nucleus (Fig 6). Separating the medial part of the lateral habenular nucleus from the mediodorsal nucleus is the dark band of the fasciculus retroflexus, which forms a distinct boundary around the ventral and medial surfaces of the habenular complex (Fig 7A).

3.1.3 *The pretectal nuclei (prosomere 1)*

The commonly recognized parts of the pretectal area are the named pretectal nuclei in the region of the posterior commissure (Figs 7B, 8A). However, each prosomere is a complete segment extending from the dorsal to the ventral surface of the neural tube and, therefore, includes many structures ventral to the posterior commissure. These include nuclei formerly classified with the midbrain - the nucleus of Darkschewitz,

the interstitial nucleus of Cajal, and the pre-Edinger-Westphal complex (Fig 8B). The most ventral part of prosomere 1 forms the rostral parts of the substantia nigra and ventral tegmental area, as do the ventral extensions of prosomeres 1 and 2. These ventral extensions are relatively slender, but can be appreciated diagrammatically in Figure 1. Most of the pretectal nuclei close to the posterior commissure are relatively small, but the anterior pretectal nucleus occupies a considerable area medial to the medial posterior nucleus and the medial geniculate nucleus (Fig 8). The area between the anterior pretectal nucleus and the periaqueductal gray is called the p1 reticular formation (Fig 8B). The rostral pole of the superior colliculus is formed by a non-laminated nucleus called the tectal gray (Puelles et al., 2012a) (Fig 8). A thin band of prosomere 1 separates the tectal gray from the medial geniculate (Fig 8B).

The FSL atlas package used by our consortium includes labels for the segmentation of the mouse diencephalon, as well as the previous AMBMC atlases including the basal ganglia (Ullmann et al., 2014), cerebellum (Ullmann et al., 2012), cerebral cortex (Ullmann et al., 2013), and hippocampus (Richards et al., 2011). Additionally, a symmetric average mouse brain MRI model is included in the package that should be used for image registrations (Janke and Ullmann, 2015). Users of this package are also provided with a configuration file, which contains the suggested parameters for performing non-linear registration of a 30 μm mouse brain T_2*-weighted MRI to the 15 μm AMBMC T_2*-weighted mouse brain model in FSL (FNIRT).

4. DISCUSSION

This paper is the fifth of a series of studies describing the detailed anatomy of major brain regions as seen in MR images based upon the Australian Mouse Brain Mapping Consortium (AMBMC) template brain. The previous papers in the series dealt with the hippocampus (Richards et al., 2011), the cerebellum (Ullmann et al., 2012), the basal ganglia (Ullmann et al., 2014), and the cerebral cortex (Ullmann et al., 2013). The present paper offers a detailed description of the major parts of the mouse diencephalon in high-resolution MR images. However, segmentation of T_2*-weighted MR images of the diencephalon is challenging; in comparison to the hippocampus, which has clear boundaries between layers, and the cerebellum, which has clear structural boundaries, many parts of the diencephalon possess relatively subtle variations in contrast. In many previous MR studies in the components of the thalamus were not identified (Dorr et al., 2008), with the study by Moldrich et al. (2010) being the only one to attempt to segment the thalamus.

The images used in this atlas have benefited from a combination of enhanced contrast obtained by perfusion with a gadolinium contrast agent, and improved signal to noise ratio produced by the average of MR scans from many animals. These factors allowed us to identify subtle differences in contrast that define adjacent structures. However, it is important to recognize the significant shortcomings associated with the segmentation process. Manual segmentation is susceptible to image quality and partial volume effects, the choice of criteria for the structural boundaries, and the level of experience of the observers. As a result, automatic segmentation based purely on available contrast is considered by some to be preferable to manual segmentation. We disagree with this opinion. In this atlas we found that the subtle differences in white matter and cell density in the diencephalon that could make automatic segmentation unrealistic. To minimize errors, we therefore utilized high-resolution data (15 μm^3)

with a high signal to noise ratio, clearly defined boundary criteria, and relied on expert anatomists with significant experience in segmentation of MR images. Manual segmentation is time consuming, so we chose to trace every 5th slice and then smooth and interpolate for intermediate slices. In cases where this did not provide sufficient detail of tracing, intermediate slices were also traced so that a contiguous final tracing was achieved. Intermediate tracings were usually required in areas where tracings of a structure did not overlap or were disjunct from the slice five sections away.

4.1 *The application of an ontology based on developmental gene expression*

As noted in the introduction, the subdivision of the diencephalon in this paper is based on recent evidence from developmental gene expression (Puelles et al., 2013). The hierarchical classification of brain structures is known as an ontology, and the most reliable current ontology is one based on developmental gene expression. Up until recently major published brain ontologies were based on traditional topographical subdivisions of the brain (e.g. Bowden et al, 2007; Bota and Swanson, 2008). These ontologies did not take into account the insights derived from developmental gene expression and so it contained many errors. The proper classification of brain structures using developmental gene expression is not just an academic exercise, since the territories defined by gene expression each determine the anatomical and physiological characteristics of the component nuclei (Puelles et al., 2013). If these developmental gene expression territories are ignored, there is a risk that future studies will misinterpret anatomical and functional relationships between nuclei. The developmental gene expression ontology shows that the hypothalamus is not part of the diencephalon, and demonstrates that each of the diencephalic prosomeres is a complete segment of the neural tube with alar and basal components.

4.2 *Using high resolution data in studies that employ lower resolution images*

This study is based on the analysis of high-resolution images of the diencephalon and we acknowledge that the vast majority of mouse MRI studies are based on much lower resolution images. The use of lower resolution images may be dictated by functional considerations, such as the need for a low-resolution time series or large-scale functional connectivity mapping. However the major landmarks we have used (particularly the large fiber bundles) are well seen in lower resolution images, and we believe taht that users will be able to match a particular image in their own data with one of our illustrations. Once a match is identified, the user will be able to reliably interpolate details of individual nuclei as required.

4.3 *Is the segmentation based on the Paxinos and Franklin atlas consistent with that seen in the Allen Reference Atlas of the mouse brain?*

The Allen Reference Atlas (Dong, 2007) provides an important competing version of mouse brain segmentation, and it is freely available on the Allen website. We have found that the detailed segmentation of the thalamus and related areas in the Dong atlas is very similar to that offered by the Paxinos and Franklin (2013) atlas. We believe that either atlas will provide a reliable guide to segmentation of the diencephalon. The only major difference is that the Dong atlas uses the traditional ontology as a basis for subdivsions instead of the new developmentally based ontology (which incidentally is used in the Allen developing mouse brain atlases).

5. CONCLUSIONS

We have used high-resolution averaged MR images to construct a detailed atlas of the diencephalon of the C57BL/6J mouse. A novel feature of this atlas is that the anatomical characterization and subdivision of the diencephalon is based on modern studies of developmental gene expression rather than traditional subdivisions based on external appearance.

Conflict of interest statement
The authors declare no conflict of interest.

ACKNOWLEGEMENTS
We thank the Queensland NMR Network (QNN) and the National Imaging Facility (NIF) for instrument access and technical support. This work was supported by the National Health and Medical Research Council (NHMRC) of Australia and the Australian National Data Service (ANDS) through the National Collaborative Research Infrastructure Strategy Program.

REFERENCES

Albu, A.B., Beugeling, T., Laurendeau, D., 2008. A morphology-based approach for interslice interpolation of anatomical slices from volumetric images. IEEE Trans Biomed Eng 55, 2022-2038.
Andersson, J., Jenkinson, M., and Smith, S. (2007). Non-linear registration, aka spatial normalisation. Technical Report TR07JA2, Oxford Centre for Functional Magnetic Resonance Imaging of the Brain, Department of Clinical Neurology, Oxford University, Oxford, UK. Available at http://www.fmrib.ox.ac.uk/analysis/techrep for downloading.
Bota, M., Swanson, L.W., 2008. BAMS neuroanatomical ontology: design and implementation. Front. Neuroinform 2, 2.
Bowden, D.M., Dubach, M., Park, J., 2007. Creating neuroscience ontologies. Methods Mol. Biol. 401, 67–87.
Dong , H.W., 2008. Allen Reference Atlas: A Digital Color Brain Atlas of the C57BL/J6 Male Mouse. John Wiley and Son, Hoboken NJ.
Dorr, A.E., Lerch, J.P., Spring, S., Kabani, N., Henkelman, R.M., 2008. High resolution three-dimensional brain atlas using an average magnetic resonance image of 40 adult C57BL/6J mice. Neuroimage 42, 60-69.
Ferris, C.F., Kulkarni, P., Toddes, S., Yee, J., Kenkel, W., Nedelman, M., 2014. Studies on the Q175 Knock-in Model of Huntington's Disease Using Functional Imaging in Awake Mice: Evidence of Olfactory Dysfunction. Front Neurol 5, 94.
Janke, A.L., Ullmann, J.F., 2015. Robust methods to create ex vivo minimum deformation atlases for brain mapping. Methods 73, 18-26.
Jenkinson, M., Beckmann, C.F., Behrens, T.E., Woolrich, M.W., Smith, S.M., 2012. FSL. Neuroimage 62, 782-790.
Jones, E.G., 2007. The Thalamus. Cambridge University Press, Cambridge.

Keifer, O.P., Jr., Gutman, D.A., Hecht, E.E., Keilholz, S.D., Ressler, K.J., 2015. A comparative analysis of mouse and human medial geniculate nucleus connectivity: A DTI and anterograde tracing study. Neuroimage 105, 53-66.
Kovacevic, N., Henderson, J.T., Chan, E., Lifshitz, N., Bishop, J., Evans, A.C., Henkelman, R.M., Chen, X.J., 2005. A three-dimensional MRI atlas of the mouse brain with estimates of the average and variability. Cereb. Cortex 15, 639-645.
Ma, Y., Hof, P.R., Grant, S.C., Blackband, S.J., Bennett, R., Slatest, L., McGuigan, M.D., Benveniste, H., 2005. A three-dimensional digital atlas database of the adult C57BL/6J mouse brain by magnetic resonance microscopy. Neuroscience 135, 1203-1215.
MacKenzie-Graham, A., Lee, E.F., Dinov, I.D., Bota, M., Shattuck, D.W., Ruffins, S., Yuan, H., Konstantinidis, F., Pitiot, A., Ding, Y., Hu, G.G., Jacobs, R.E., Toga, A.W., 2004. A multimodal, multidimensional atlas of the C57BL/6J mouse brain. J Anat 204, 93-102.
Maheswaran, S., Barjat, H., Rueckert, D., Bate, S.T., Howlett, D.R., Tilling, L., Smart, S.C., Pohlmann, A., Richardson, J.C., Hartkens, T., Hill, D.L., Upton, N., Hajnal, J.V., James, M.F., 2009. Longitudinal regional brain volume changes quantified in normal aging and Alzheimer's APP x PS1 mice using MRI. Brain Res 1270, 19-32.
Malkova, N.V., Gallagher, J.J., Yu, C.Z., Jacobs, R.E., Patterson, P.H., 2014. Manganese-enhanced magnetic resonance imaging reveals increased DOI-induced brain activity in a mouse model of schizophrenia. Proc Natl Acad Sci U S A 111, E2492-2500.
Moldrich, R.X., Pannek, K., Hoch, R., Rubenstein, J.L., Kurniawan, N.D., Richards, L.J., 2010. Comparative mouse brain tractography of diffusion magnetic resonance imaging. Neuroimage 51, 1027-1036.
Nessler, S., Boretius, S., Stadelmann, C., Bittner, A., Merkler, D., Hartung, H.P., Michaelis, T., Bruck, W., Frahm, J., Sommer, N., Hemmer, B., 2007. Early MRI changes in a mouse model of multiple sclerosis are predictive of severe inflammatory tissue damage. Brain 130, 2186-2198.
Oh, S.W., Harris, A., Ng, L., et al. (2014) A mesoscale connectome of the mouse brain, Nature 508: 207-214. doi:10.1038/nature13186.
Paxinos, G., Franklin, K., 2013. The Mouse Brain in Stereotaxic Coordinates, 4th edn. Elsevier Academic Press, San Diego.
Paxinos, G., Watson, C., 2014. Paxinos and Watson's The Rat Brain in Stereotaxic Coordinates, 7th edn. Elsevier Academic Press, San Diego.
Paxinos, G., Watson, C., Carrive, P., Kirkcaldie, M.T., Ashwell, K., 2009. Chemoarchitectonic Atlas of the Rat Brain. Elsevier Academic Press, San Diego.
Puelles, L., Harrison, M., Paxinos, G., Watson, C., 2013. A developmental ontology for the mammalian brain based on the prosomeric model. Trends Neurosci 36, 570-578.
Puelles, E., Martinez-de-la-Torre, Watson, C., Puelles, L. 2012a. Midbrain. In: Watson, C., Paxinos, G., Puelles, L. (Eds.), The Mouse Nervous System. Elsevier Academic Press, San Diego, pp337-359.
Puelles, L., Martinez-de-la-Torre, M., Ferran, J-L., Watson, C., 2012b. Diencephalon. In: Watson, C., Paxinos, G., Puelles, L. (Eds.), The Mouse Nervouse System. Elsevier Academic Press, San Diego, 313-336.
Richards, K., Calamante, F., Tournier, J.D., Kurniawan, N.D., Sadeghian, F., Retchford, A.R., Jones, G.D., Reid, C.A., Reutens, D.C., Ordidge, R., Connelly, A., Petrou, S., 2014. Mapping somatosensory connectivity in adult mice using

diffusion MRI tractography and super-resolution track density imaging. Neuroimage 102 Pt 2, 381-392.
Richards, K., Watson, C., Buckley, R.F., Kurniawan, N.D., Yang, Z., Keller, M.D., Beare, R., Bartlett, P.F., Egan, G.F., Galloway, G.J., Paxinos, G., Petrou, S., Reutens, D.C., 2011. Segmentation of the mouse hippocampal formation in magnetic resonance images. Neuroimage 58, 732-740.
Shu, X., Qin, Y.Y., Zhang, S., Jiang, J.J., Zhang, Y., Zhao, L.Y., Shan, D., Zhu, W.Z., 2013. Voxel-based diffusion tensor imaging of an APP/PS1 mouse model of Alzheimer's disease. Mol Neurobiol 48, 78-83.
Ullmann, J.F., Cowin, G., Kurniawan, N.D., Collin, S.P., 2010a. A three-dimensional digital atlas of the zebrafish brain. Neuroimage 51, 76-82.
Ullmann, J.F., Janke, A.L., Reutens, D., Watson, C., 2015. Development of MRI-based atlases of non-human brains. J Comp Neurol 523, 391-405.
Ullmann, J.F., Keller, M.D., Watson, C., Janke, A.L., Kurniawan, N.D., Yang, Z., Richards, K., Paxinos, G., Egan, G.F., Petrou, S., Bartlett, P., Galloway, G.J., Reutens, D.C., 2012. Segmentation of the C57BL/6J mouse cerebellum in magnetic resonance images. Neuroimage 62, 1408-1414.
Ullmann, J.F., Watson, C., Janke, A.L., Kurniawan, N.D., Paxinos, G., Reutens, D.C., 2014. An MRI atlas of the mouse basal ganglia. Brain Structure and Function 219, 1343-1353.
Ullmann, J.F., Watson, C., Janke, A.L., Kurniawan, N.D., Reutens, D.C., 2013. A segmentation protocol and MRI atlas of the C57BL/6J mouse neocortex. Neuroimage 78, 196-203.
Ullmann, J.F.P., Cowin, G., Collin, S.P., 2010b. Magnetic resonance microscopy of the barramundi (*Lates calcarifer*) brain. J Morph 271, 1446-1456.
Watson, C., Mitchelle, A., Puelles, L. (2017) A new mammalian brain ontology based on developmental gene expression. In Kaas J, Evolution of Nervous Systems 2 edn. Elsevier, Oxford, Vol 2 pp 53-75.
Watson, C., Paxinos, G., 2010. Chemoarchitectonic atlas of the mouse brain. Elsevier Academic Press, San Diego.

Figure 1. Six diagrams of a medial to lateral series of sagittal sections through the mouse diencephalon. In each case the distance from the midline is indicated. Prosomere 1 is colored green, prosomere 2 is colored pink, and prosomere 3 is colored yellow. The diagrams are based on drawings of sagittal sections in the mouse brain atlas of Paxinos and Franklin (2013). The abbreviations and their full names are listed in Table 1.

Figure 2. Four further diagrams that complete a series of a medial to lateral series of sagittal sections through the mouse diencephalon. In each case the distance from the midline is indicated. Prosomere 1 is colored green, prosomere 2 is colored pink, and prosomere 3 is colored yellow. The diagrams are based on drawings of sagittal sections in the mouse brain atlas of Paxinos and Franklin (2013). The abbreviations and their full names are listed in Table 1.

Figure 3. A diagram showing a dorsolateral view of the main groups of thalamic nuclei in the mouse. Rostral is to the right and the midline is at the top margin. Groups shown here are the ventral tier (ventral anterior - VA, ventral lateral -VL, ventral posterior - VP, dorsal lateral geniculate - DLG, and medial geniculate - MG), dorsal tier (lateral dorsal - LD and lateral posterior - LP), mediodorsal group (MD), anterior group (Ant), posterior group (Po), and the intralaminar-midline group (midline - ML, intralaminar - IL, and parafascicular - PaF). The position of prosomere 1 (p1) at the caudal end of the thalamus is shown.

Figure 4. (A) Three dimensional renderings of fiber-bundles used as landmarks to navigate the mouse diencephalon. (B) Three dimensional renderings of major ventral tier thalamic nuclei - the dorsal lateral geniculate nucleus, medial geniculate nucleus, and ventral thalamic nucleus.

Figure 5. **A)** An image of a coronal slice through an MR scan based on an average of eighteen mouse brains. This slice is numbered #500 in our series and is very similar to the coronal section in Fig 37 in the mouse brain atlas of Paxinos and Franklin (2013). On the right hand side of the image the major diencephalic structures have been outlined as described in the text. The main prosomere 2 structures at this level are the nuclei of the anterior group, the lateral dorsal nucleus, the habenula complex and the stria medullaris, the dorsal medial nucleus, and the intralaminar and midline nuclei. Prosomere 3 structures seen here are the zona incerta and the reticular nucleus. The hypothalamus is represented by the paraventricular nucleus and the fornix. **B)** An image of a coronal slice through an MR scan based on an average of eighteen mouse brains. This slice is numbered #509 in our series and is very similar to the coronal section in Fig 38 in the mouse brain atlas of Paxinos and Franklin (2013). The main prosomere 2 structures at this level are the nuclei of the anterior group, the lateral dorsal nucleus, the ventral anterior nucleus, the ventral medial nucleus, the habenula complex, the dorsal medial nucleus, and the intralaminar and midline nuclei. Prosomere 3 structures seen here are the zona incerta and the reticular nucleus. The hypothalamus is represented by the paraventricular nucleus and the fornix. The abbreviations and their full names are listed in Table 1.

Figure 6. **A)** An image of a coronal slice through an MR scan based on an average of eighteen mouse brains. This slice is numbered #525 in our series and is very similar to the coronal section in Fig 41 in the mouse brain atlas of Paxinos and Franklin 2013. On the right hand side of the image the major diencephalic structures have been outlined as described in the text. The main prosomere 2 structures at this level are the lateral dorsal nucleus, the ventroposterior medial and ventroposterior lateral nuclei, the ventral medial nucleus, the habenula complex and the fasciculus retroflexus, the parafascicular nucleus, the dorsal medial nucleus, and the intralaminar and midline nuclei. Prosomere 3 structures seen here are the zona incerta and the reticular nucleus. The hypothalamus is represented by the entopeduncular nucleus, the posterior part of the paraventricular nucleus, and the fornix. **B)** An image of a coronal slice through an MR scan based on an average of eighteen mouse brains. This slice is numbered #533 in our series and is very similar to the coronal section in Fig 42 in the mouse brain atlas of Paxinos and Franklin 2013). The main prosomere 2 structures at this level are the lateral dorsal nucleus, the ventral lateral nucleus, the ventroposterior medial and ventroposterior lateral nuclei, the ventral medial nucleus, the habenula complex, the

dorsal medial nucleus, and the intralaminar and midline nuclei. Prosomere 3 structures seen here are the zona incerta and the reticular nucleus. The hypothalamus is represented by the entopeduncular nucleus, the paraventricular nucleus, and the fornix. The abbreviations and their full names are listed in Table 1.

Figure 7. **A)** An image of a coronal slice through an MR scan based on an average of eighteen mouse brains. This slice is numbered #555 in our series and is very similar to the coronal section in Fig 45 in the mouse brain atlas of Paxinos and Franklin (2013). On the right hand side of the image the major diencephalic structures have been outlined as described in the text. The main prosomere 2 structures at this level are the lateral posterior nucleus, the lateral dorsal nucleus, the ventral lateral nucleus, the dorsal lateral geniculate nucleus, the ventroposterior medial and ventroposterior lateral nuclei, the ventral medial nucleus, the habenula complex and the fasciculus retroflexus, the posterior medial nucleus, the dorsal medial nucleus, the submedius nucleus, and the intralaminar and midline nuclei. Prosomere 3 structures seen here are the zona incerta and the reticular nucleus. The hypothalamus is represented by the entopeduncular nucleus, the third ventricle, and the fornix. **B)** An image of a coronal slice through an MR scan based on an average of eighteen mouse brains. This slice is numbered #576 in our series and is very similar to the coronal section in Fig 49 in the mouse brain atlas of Paxinos and Franklin (2013). Prosomere 1 structures seen here are the anterior pretectal nucleus, and the rostral tip of the posterior commissure. The main prosomere 2 structures at this level are the dorsal lateral geniculate nucleus, the posterior medial nucleus, the ventroposterior medial and ventroposterior lateral nuclei, the ventral medial nucleus, the lateral posterior nucleus, the fasciculus retroflexus, the parafascicular nucleus, and the medial lemniscus. Prosomere 3 structures seen here are the zona incerta and the pregeniculate nucleus. The hypothalamus is represented by the nucleus gemini, the subthalamic nucleus, the parasubthalamic nucleus, the terete nucleus, and the fornix. The abbreviations and their full names are listed in Table 1.

Figure 8. **A)** An image of a coronal slice through an MR scan based on an average of eighteen mouse brains. This slice is numbered #605 in our series and is very similar to the coronal section in Fig 53 in the mouse brain atlas of Paxinos and Franklin (2013). On the right hand side of the image the major diencephalic structures have been outlined as described in the text. Prosomere 1 structures seen here are the anterior pretectal nucleus, the nuclei associated with the posterior commissure, and the posterior commissure itself. The prosomere 2 structures at this level the dorsal lateral geniculate nucleus, members of the posterior group, the caudal ventroposterior medial nucleus, and the caudal pole of the lateral posterior nucleus, the fasciculus retroflexus, the parafascicuar nucleus, and the auditory radiation. Prosomere 3 structures seen here are the zona incerta, the pregeniculate nucleus, the subgeniculate nucleus and the rostral part of the substantia nigra. The midbrain is represented by parts of the superior colliculus and the tectal gray. **B)** An image of a coronal slice through an MR scan based on an average of eighteen mouse brains. This slice is numbered #637 in our series and is very similar to the coronal section in Fig 56 in the mouse brain atlas of Paxinos and Franklin (2013). The major diencephalic structures have been outlined as described in the text. Prosomere 1 structures seen here are the anterior pretectal nucleus, the pre-Edinger-Westphal nucleus, the nucleus of Darkschewitsch, the interstitial nucleus of Cajal and its shell, and the posterior commissure. The prosomere 2 structures at this level the medial geniculate nucleus, and the members of

the posterior group. Prosomere 3 structures seen here are the caudal zona incerta, and rostral parts of the substantia nigra and VTA. The remaining structures belong to the midbrain. The abbreviations and their full names are listed in Table 1.

Highlights

- A detailed atlas of high resolution images of the diencephalon of the adult C57Bl/6J mouse
- The atlas is based on data from an average of 18 brains imaged with a 16.4T MR scanner
- The MRI atlas is the first to be based on a modern developmental ontology of the diencephalon
- This atlas is available for download at www.imaging.org.au/AMBMC.
- The atlas is accompanied by an FSL package to enable nonlinear registration of novel data sets to the AMBMC model and subsequent automatic segmentation

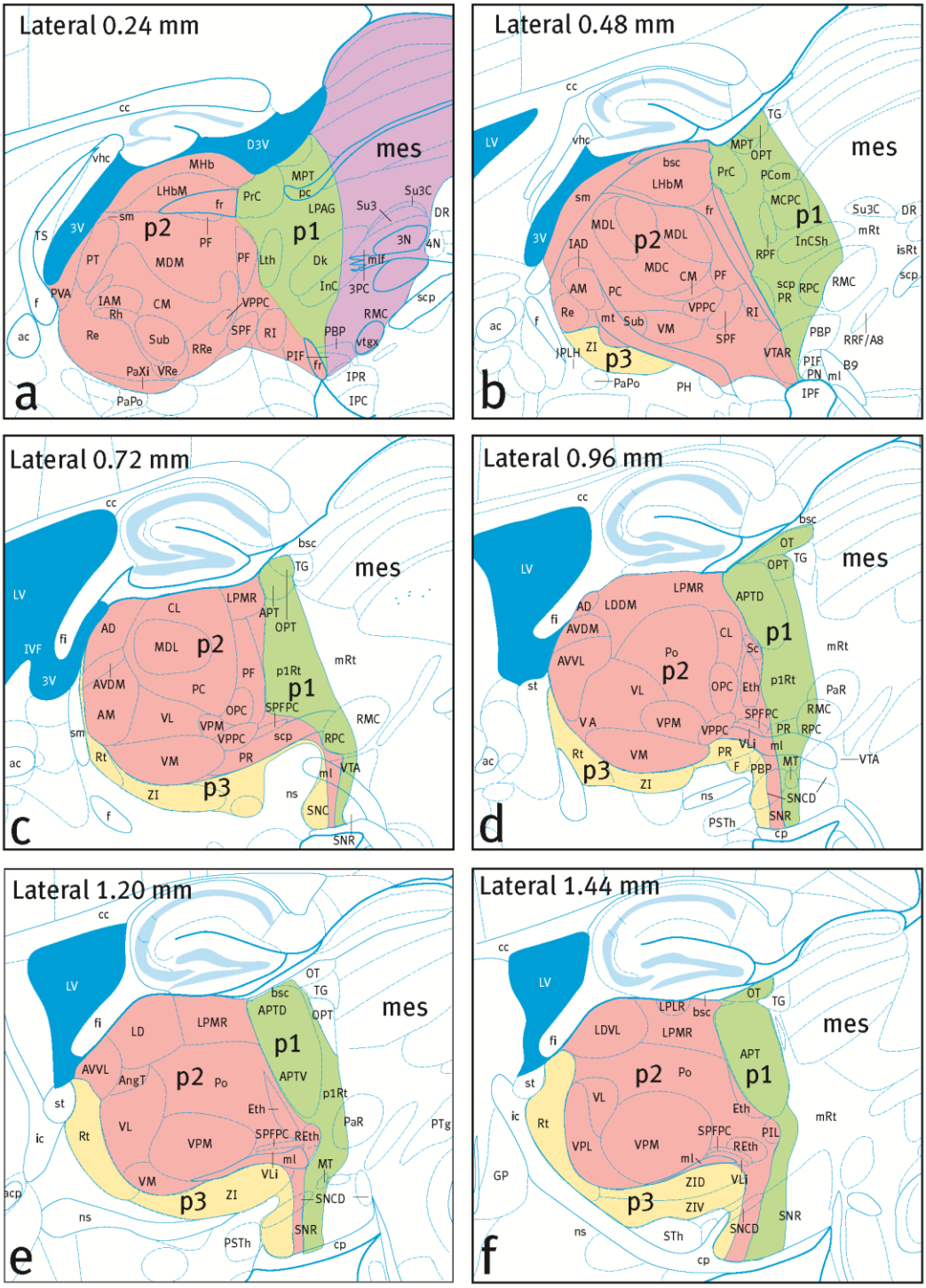

fig1

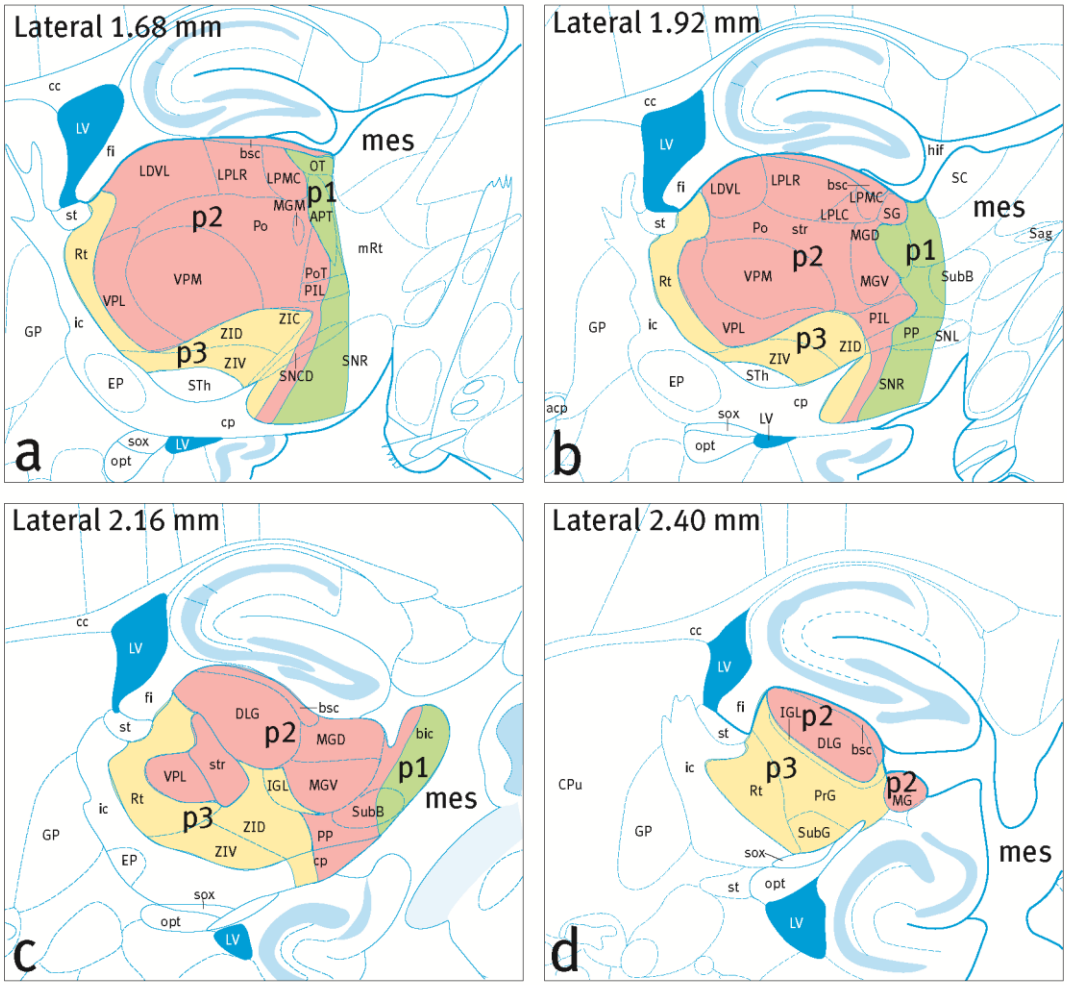

fig2

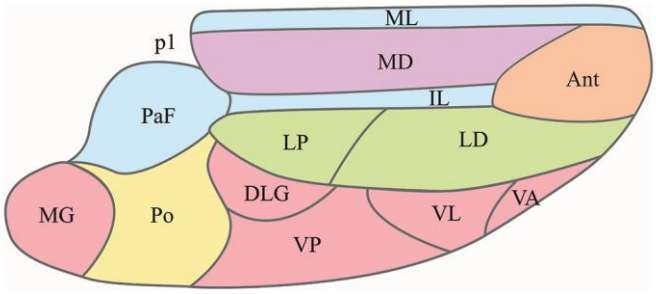

fig3

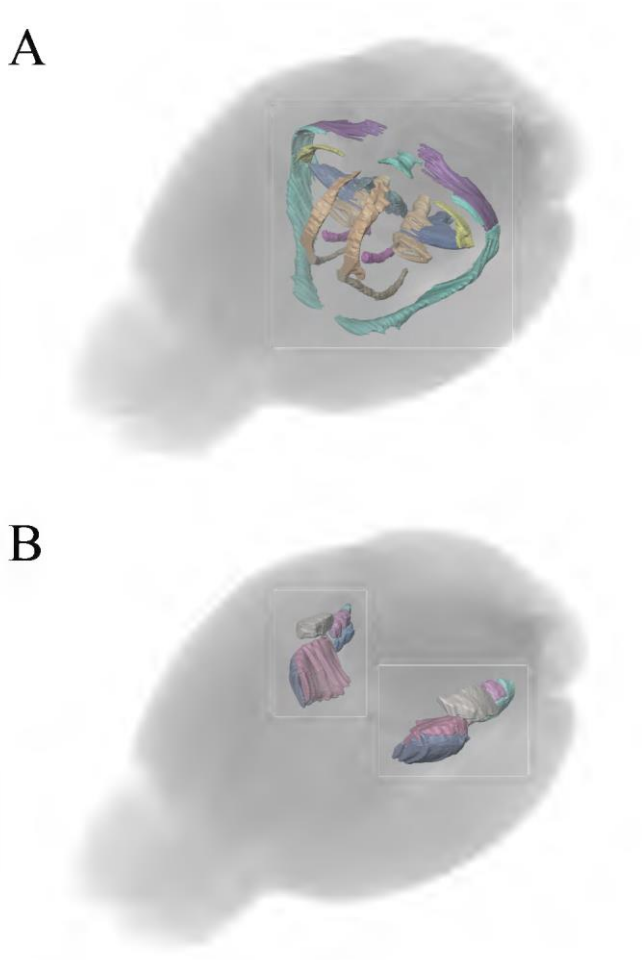

fig4

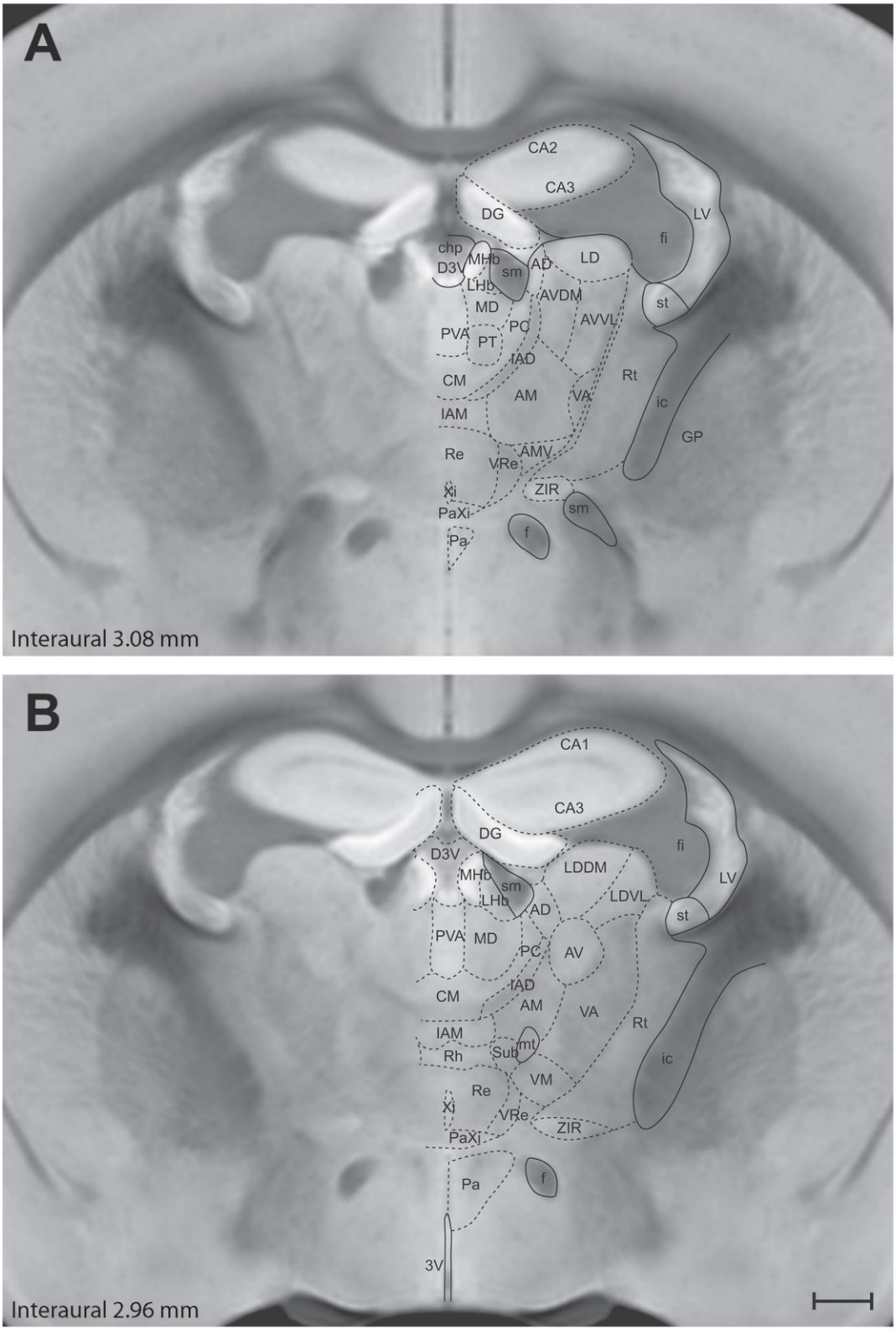
A
CA2
CA3
DG
LV
fi
chp
MHb
D3V
AD
LD
sm
LHb
AVDM
st
MD
PC
AVVL
PVA
PT
IAD
CM
Rt
AM
VA
ic
IAM
GP
Re
AMV
VRe
ZIR
Xi
PaXi
sm
Pa
f
Interaural 3.08 mm
B
CA1
CA3
DG
fi
D3V
LDDM
MHb
sm
LV
LHb
LDVL
AD
st
PVA
MD
PC
AV
IAD
CM
AM
VA
Rt
IAM
mt
Rh
Sub
ic
VM
Re
Xi
VRe
ZIR
PaXi
Pa
f
3V
Interaural 2.96 mm

fig5

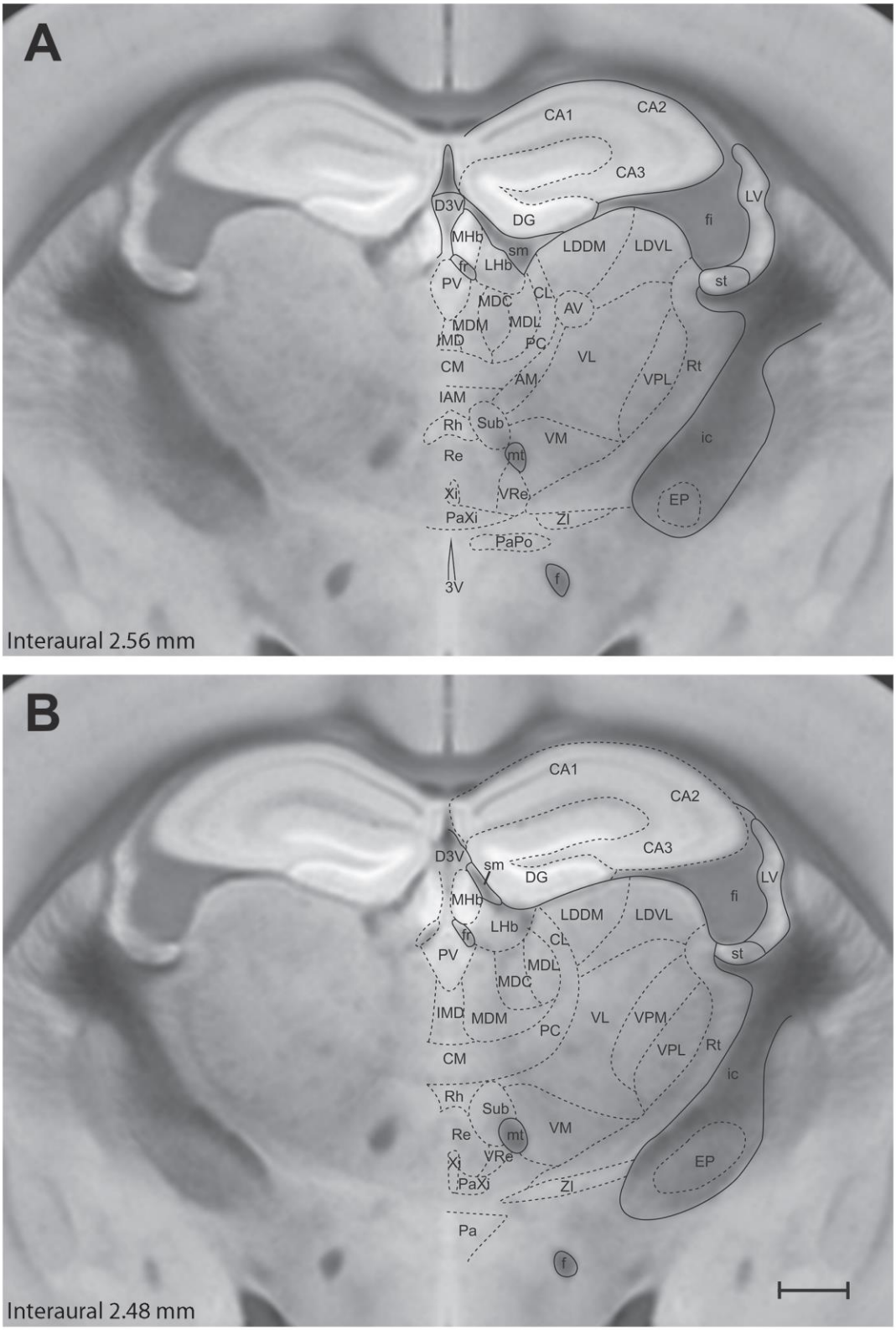
A
CA1
CA2
CA3
D3V
DG
LV
fi
MHb
sm
LDDM
LDVL
fr
LHb
st
PV
CL
MDC
AV
MDM
MDL
IMD
PC
VL
CM
AM
VPL
Rt
IAM
Rh
Sub
VM
ic
Re
mt
Xi
VRe
EP
PaXi
ZI
PaPo
3V
f
Interaural 2.56 mm
B
CA1
CA2
CA3
D3V
sm
DG
LV
fi
MHb
LDDM
LDVL
LHb
fr
CL
PV
st
MDL
MDC
IMD
MDM
VL
VPM
PC
VPL
Rt
CM
ic
Rh
Sub
VM
Re
mt
Xi
VRe
EP
PaXi
ZI
Pa
f
Interaural 2.48 mm

fig6

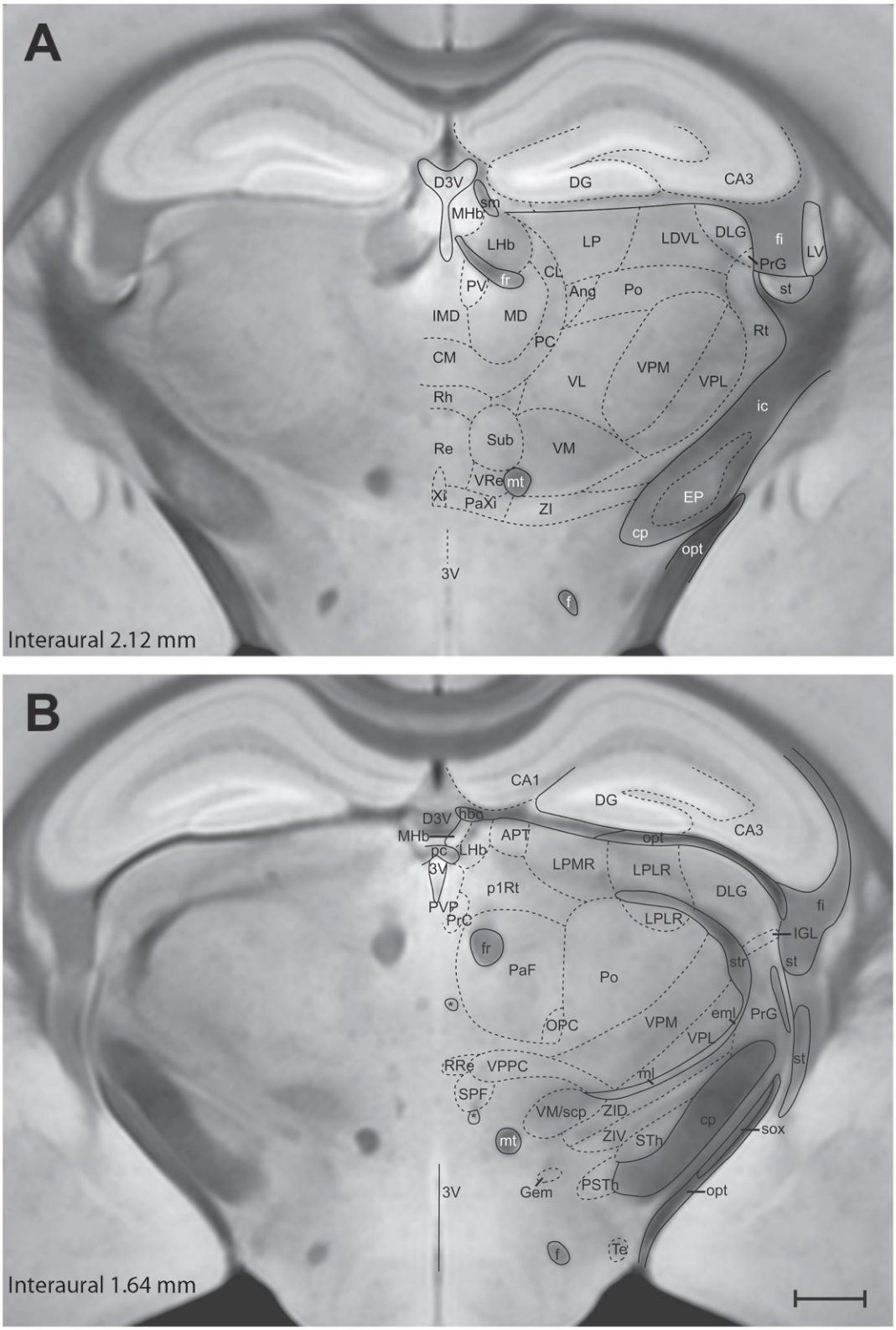
A
D3V
DG
CA3
sm
MHb
LHb
LP
LDVL
DLG
fi
LV
PrG
st
PV
fr
CL
Ang
Po
IMD
MD
PC
Rt
CM
VPM
VPL
VL
Rh
ic
Re
Sub
VM
VRe
mt
Xi
PaXi
ZI
EP
cp
opt
3V
f
Interaural 2.12 mm
B
CA1
DG
D3V
hbc
CA3
MHb
APT
opt
pc
LHb
LPMR
LPLR
3V
p1Rt
DLG
fi
PVP
PrC
LPLR
IGL
fr
str
st
PaF
Po
OPC
VPM
eml
PrG
VPL
st
RRe
VPPC
ml
SPF
VM/scp
ZID
cp
sox
mt
ZIV
STh
3V
Gem
PSTh
opt
f
Te
Interaural 1.64 mm

fig7

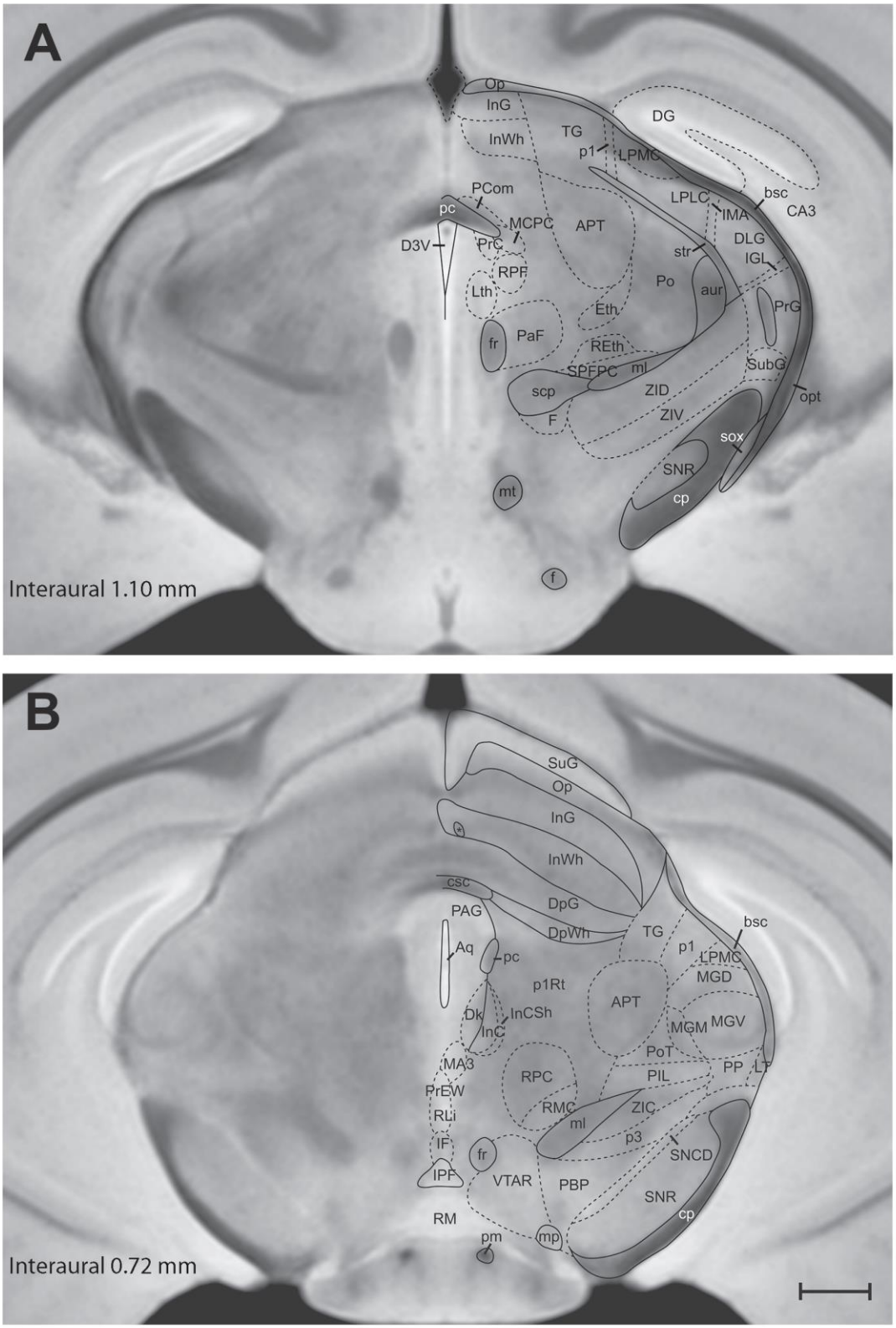
A
Op
lnG
lnWh
TG
p1
LPMC
DG
PCom
pc
MCPC
APT
LPLC
IMA
bsc
CA3
D3V
PrC
RPF
Lth
str
DLG
IGL
Po
aur
Eth
PrG
fr
PaF
REth
SPFPC
ml
SubG
scp
ZID
opt
F
ZIV
sox
SNR
mt
cp
f
Interaural 1.10 mm
B
SuG
Op
lnG
lnWh
csc
DpG
PAG
DpWh
TG
bsc
Aq
pc
p1
LPMC
p1Rt
MGD
APT
Dk
lnCSh
MGM
MGV
lnC
PoT
MA3
RPC
PIL
PP
LT
PrEW
RMC
ZIC
RLi
ml
IF
fr
p3
SNCD
IPF
VTAR
PBP
SNR
RM
cp
pm
mp
Interaural 0.72 mm

Fig8